

## Preparation and Electrochemical Performance of Manganese-Doped Nickel Hydroxide Cathode Materials

Min Xiao<sup>1</sup>, Fei Dou<sup>1,2</sup>, Shouguang Yao<sup>1,\*</sup>, Ruyue Xing<sup>1,2</sup>, Jie Cheng<sup>2,3</sup>, Yusheng Yang<sup>2,3</sup>

<sup>1</sup> School of Energy and Power Engineering, Jiangsu University of Science and Technology, Zhenjiang, Jiangsu 212003, China

<sup>2</sup> Zhangjiagang Smartgrid Fanghua electrical energy storage research institute Co. Ltd., Zhangjiagang 215600, China

<sup>3</sup> Chilwee Power Co., Ltd., Huzhou 313100, China

\*E-mail: [zjyaosg@126.com](mailto:zjyaosg@126.com)

Received: 3 March 2020 / Accepted: 8 May 2020 / Published: 10 June 2020

Buffer solution method can maintain the stability of pH in the reaction process, so that the physical and chemical properties of the product are good. Manganese-doped  $\text{Ni}_{1-x}\text{Mn}_x(\text{OH})_2$  ( $x=0.15, 0.18, 0.22, 0.25$ ) was prepared by buffer solution method. X-ray diffraction measurements showed that the samples were mainly composed of  $\beta\text{-Ni}(\text{OH})_2$ , and some of the Mn-doped samples contain a small amount of impurities. Scanning electron microscopy measurements showed that the crystal particles of Mn-doped samples were small. The specific surface area measurements results showed that the BET surface area of Mn-doped samples were more and the Mn-doped samples had mesoporous structures. Cyclic voltammetry results showed that the difference between the oxidation peak potential and the reduction peak potential of the Mn-doped samples was small. The Mn-doped samples demonstrated better electrochemical performance than commercial  $\beta\text{-Ni}(\text{OH})_2$ . Constant current charge-discharge results showed that samples with an Mn content of 18 mol% yielded the highest discharge specific capacity, the best cycle stability with discharge specific capacity of  $314.5 \text{ mAh g}^{-1}$  at  $800 \text{ mA g}^{-1}$ , while the discharge specific capacity of commercial  $\beta\text{-Ni}(\text{OH})_2$  was  $195 \text{ mAh g}^{-1}$ . It shows that Mn doping can improve the discharge specific capacity of the positive electrode and make the battery have good charge and discharge performance at high current. When the sample with Mn content of 18 mol% was cycled at  $800 \text{ mA g}^{-1}$  for 30 cycles, the discharge specific capacity did not decrease, while other samples containing Mn and commercial  $\beta\text{-Ni}(\text{OH})_2$  showed different degrees of discharge specific capacity. As a positive electrode material,  $\text{Ni}_{0.82}\text{Mn}_{0.18}(\text{OH})_2$  has good cycle stability. A series of experimental results have proved that a proper amount of Mn doping (18 mol%) can effectively improve the electrochemical performance of nickel electrodes and reduce the cost of cathode materials.

**Keywords:** Buffer solution method; Mn-doped  $\text{Ni}(\text{OH})_2$ ; Rate capability; Cyclic stability

## 1. INTRODUCTION

Zinc–nickel battery is a green and environmentally friendly chemical power source. Compared with the potential environmental hazards of traditional lead–acid batteries [1] and nickel–cadmium batteries [2,3], as well as the high cost of manufacturing nickel–metal hydride batteries [4], zinc–nickel batteries are safer, more environmentally friendly, and more economical. The zinc–nickel battery may be an ideal chemical power source to replace traditional lead–acid batteries and nickel–cadmium batteries. In 2007, Cheng Jie's group presented a zinc–nickel single-liquid battery with a sintered nickel electrode as the positive electrode [5,6]. This type of battery solves the problem of zinc dendrite by flowing the electrolyte and controlling zinc deposition/dissolution. The electrolyte containing ZnO can stabilize the crystal structure of Ni(OH)<sub>2</sub> [7], and the cycle life is greatly improved, but the overall specific energy of the battery is lowered, The research team used several methods to improve its performance [8].

To increase the specific capacity of zinc–nickel batteries, scholars have adopted a method of doping metal ions on nickel electrodes and obtained some encouraging results. Chang Yanqin's group prepared nanosheet Mn-doped  $\alpha$ -Ni(OH)<sub>2</sub> by chemical co-precipitation [9], and they found that its electrochemical performance changes with the increase in the Mn content. When the Mn content was 30 mol%, the electrochemical performance was the best, and its specific capacity was 330 mAh·g<sup>-1</sup>. Wu Meiyin's group prepared a sample of Mn-doped Ni(OH)<sub>2</sub> by chemical co-precipitation [10]. When the Mn content reached 28.3 mol%,  $\alpha$ -Ni(OH)<sub>2</sub> was obtained. At the current of 1 C, the discharge specific capacity was 190 mAh·g<sup>-1</sup> after five cycles, and the discharge specific capacity increased to 270 mAh·g<sup>-1</sup> after 300 cycles. Li Xiaofeng's group used mechanical ball milling to prepare Mn-doped  $\beta$ -Ni(OH)<sub>2</sub> [11], and the specific capacity decreased with the increase in the Mn doping amount. The highest specific capacity of the Ni<sub>0.8</sub>Mn<sub>0.2</sub>(OH)<sub>2</sub> sample was 261 mAh·g<sup>-1</sup>. When Mn and Zn co-doped Ni(OH)<sub>2</sub> were prepared by mechanical ball milling [12], the phase structure of Ni<sub>0.8</sub>Mn<sub>0.2-y</sub>Zn<sub>y</sub>(OH)<sub>2</sub> (y=0–0.075) was  $\beta$ -type. The sample Ni<sub>0.8</sub>Mn<sub>0.15</sub>Zn<sub>0.05</sub>(OH)<sub>2</sub> had a discharge specific capacity of 265 mAh·g<sup>-1</sup> at a current of 0.2 C, and the current performance of the Mn- and Zn-doped samples was high. Wen Shengshan's group prepared a sample of Al-substituted Ni in Ni(OH)<sub>2</sub> by chemical coprecipitation [13]. They reported that the Al-doped sample has higher electrochemical activity than the undoped Al sample. When the Al content was 15 mol%, the mass specific capacity was up to 324 mAh·g<sup>-1</sup> at a constant current charge and discharge of 100 mA·g<sup>-1</sup>. Jie Bao's group synthesized Cu single-doped and Cu/Al co-doped nickel hydroxide by ultrasonic-assisted precipitation [14]. Their results indicated that the electrochemical performance of Cu/Al co-doped nano-nickel hydroxide is better than that of Cu single-doped nano-nickel hydroxide. The discharge specific capacity of Cu/Al co-doped nano-nickel hydroxide reached 330 mAh·g<sup>-1</sup> at 0.2 C, which was 12 mAh·g<sup>-1</sup> more than that of Cu single-doped sample and 91 mAh·g<sup>-1</sup> more than that of pure spherical nickel hydroxide. Xue's group prepared a nanofibrous Co-substituted Ni in  $\alpha$ -Ni(OH)<sub>2</sub> by hydrothermal synthesis [15]. Their results showed that the nanofibrous structure of the sample can reduce the electrochemical reaction resistance of the electrode. In addition, at a molar Co content of 11.1%,  $\alpha$ -Ni(OH)<sub>2</sub> showed an increase in its discharge specific capacity.

Previous studies revealed that doping Mn in Ni(OH)<sub>2</sub> can improve the electrochemical performance of the Ni electrode [9-12, 16-19]. However, in the  $\beta$  structure, the discharge specific

capacity increases slightly, which may be due to the fact that ball milling is not conducive to improving the performance of Ni(OH)<sub>2</sub> material. Buffer solution method can maintain the stability of pH in the reaction process, so that the physical and chemical properties of the product are good. The literature showed that Mn-doped Ni(OH)<sub>2</sub> prepared by buffer solution method presents good electrochemical performance [16]. When the Mn content is 20 mol%, the discharge specific capacity can reach 271.8 mAh·g<sup>-1</sup>. In the present study, the Mn content was refined on the basis of the literature [16], and Ni<sub>1-x</sub>Mn<sub>x</sub>(OH)<sub>2</sub> (x=0.15, 0.18, 0.22, 0.25) was prepared by buffer solution method. Commercial β-Ni(OH)<sub>2</sub> was used as a comparison, and the electrochemical performance was found to be the best when the Mn content was 18 mol%.

## 2. EXPERIMENTAL SECTION

### 2.1. Material Synthesis

Ni<sub>1-x</sub>Mn<sub>x</sub>(OH)<sub>2</sub> (x=0.15, 0.18, 0.22, 0.25) was prepared by buffer solution method [20,21]. First, a buffer solution was prepared by dissolving 5.4 g of ammonium chloride in distilled water. About 35 mL of ammonia water was added to the mixture until a constant volume of 100 mL was obtained. The pH of the solution was about 10. Second, on the basis of the molar ratios of Ni and Mn at 85:15, 82:18, 78:22, and 75:25, appropriate amounts of NiSO<sub>4</sub>·6H<sub>2</sub>O and MnSO<sub>4</sub>·H<sub>2</sub>O were dissolved in 200 mL of distilled water; thus, solution 1 was prepared. Solution 2 was obtained by dissolving 16 g NaOH in 200 mL of deionized water. Third, under magnetic stirring, 1–2 drops of solution were added to three flasks containing buffer solution. The feeding speed was controlled to 5 mL·min<sup>-1</sup>, and the reaction temperature was set to 55 °C. Thereafter, the mixture continued to react for 8 h under strong stirring and allowed to age for 10 h at 60 °C. The mixture was filtered and washed to neutrality with warm deionized water. The samples were dried in a vacuum drying chamber at 60 °C to a constant weight and then milled in a ball mill at 400 r·min<sup>-1</sup> for 4 h to form powder samples.

The Ni<sub>1-x</sub>Mn<sub>x</sub>(OH)<sub>2</sub> sample, graphite emulsion (alcohol soluble, 30wt% solid content), and nickel powder were mixed in a 3:1:1 ratio and then added with an appropriate amount of anhydrous alcohol. After grinding for 30 min by an agate mortar, the slurry was coated on 2 cm×2 cm foam nickel. After drying at 60 °C for 4 h, another 2 cm×2 cm foam nickel was used to cover the coating with slurry. The nickel electrode was prepared by compacting it on a powder tablet press at 20 MPa.

### 2.2. Material characterizations

X-ray diffraction (XRD; D/Max-3B, Cu Kα) was conducted to analyze the crystal structures of the Ni<sub>1-x</sub>Mn<sub>x</sub>(OH)<sub>2</sub> samples. The working conditions were as follows: λ=0.1542 nm, tube pressure of 40 kV, tube flow of 30 mA, scan rate of 2 degree min<sup>-1</sup>, and scanning range of 2θ=10°–80°. The surface morphology of Ni<sub>1-x</sub>Mn<sub>x</sub>(OH)<sub>2</sub> was observed by scanning electron microscopy (SEM). The working voltage was 2 kV.

### 2.3. Electrochemical measurements

A beaker-type and two-electrode test system was developed with 2 cm×2 cm stainless steel strip as negative electrode and 10 mol·L<sup>-1</sup> KOH+1 mol·L<sup>-1</sup> ZnO+20 g·L<sup>-1</sup> LiOH mixed solution as electrolyte [16]. Constant current charging and discharging tests were carried out on the LAND battery test system. The current density was 100, 150, 200, 300, 500, and 800 mA·g<sup>-1</sup>. The charging cut-off conditions were a capacity of 320 mAh·g<sup>-1</sup> or cut-off voltage of 2.2 V and discharge cut-off voltage of 1.2 V.

A three-electrode test system was constructed using mercury oxide electrode as reference electrode. The cyclic voltammetry (CV) test was carried out at a CHI608E electrochemical workstation. The scan rate was 0.5 mV·s<sup>-1</sup>, and the voltage range was 0–0.7 V (vs. Hg/HgO).

## 3. RESULTS AND DISCUSSION

### 3.1 Phase analysis

Fig. 1 shows the XRD patterns of commercial  $\beta$ -Ni(OH)<sub>2</sub> and Ni<sub>1-x</sub>Mn<sub>x</sub>(OH)<sub>2</sub> (x=0.15, 0.18, 0.22, 0.25). By comparing the standard chart (PDF14-0117), the diffraction peaks at 2 $\theta$ =19.03°, 33.18°, 38.54°, 51.85°, 59.04°, and 62.70° were observed in the figure, corresponding to crystal faces (001), (100), (101), (102), (110), and (111), respectively. All five samples showed typical  $\beta$ -Ni(OH)<sub>2</sub> structural features, and Mn doping did not change the crystal structure of Ni(OH)<sub>2</sub>. The diffraction peaks of samples x=0.18, x=0.22, and x=0.25 at 2 $\theta$ =35.99° were consistent with the (211) crystal plane of Mn<sub>3</sub>O<sub>4</sub> (PDF04-0732), indicating the presence of Mn<sub>3</sub>O<sub>4</sub> impurities, which were presumed to be due to the oxidation of manganese ions in solution 1. In Fig. 1, as the amount of Mn doping decreased, the peak shape became increasingly sharp, and the half-width of Ni<sub>1-x</sub>Mn<sub>x</sub>(OH)<sub>2</sub> became narrow. According to the X-ray Scherrer formula  $\beta=K\lambda/D\cos\theta$ , the half-width  $\beta$  is inversely proportional to the grain size D of the powder, and the grain size of Ni<sub>1-x</sub>Mn<sub>x</sub>(OH)<sub>2</sub> gradually increases as the amount of Mn doping decreases. Thus, the substitution of Mn refines the grain of the material, and the fine grain size of nickel hydroxide powder leads to improved electrical properties [22,23].

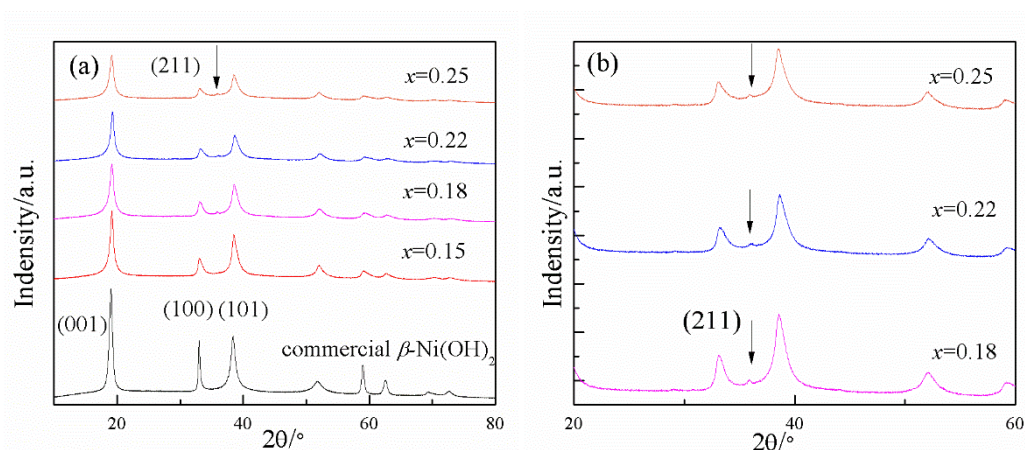


**Figure 1.** XRD patterns of commercial  $\beta$ -Ni(OH)<sub>2</sub> and Ni<sub>1-x</sub>Mn<sub>x</sub>(OH)<sub>2</sub> (x=0.15, 0.18, 0.22, 0.25);

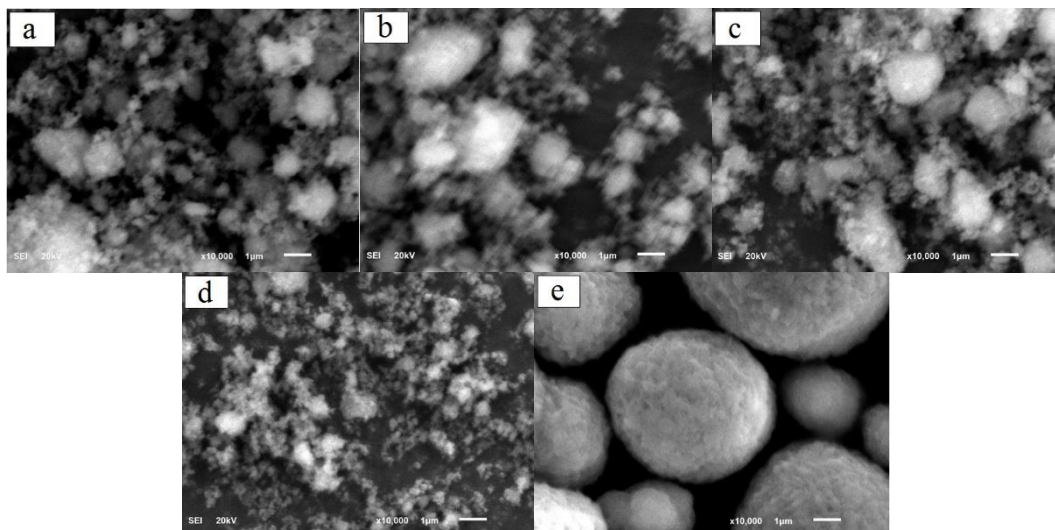


**Figure 2.** SEM images of commercial  $\beta$ -Ni(OH)<sub>2</sub> and Ni<sub>1-x</sub>Mn<sub>x</sub>(OH)<sub>2</sub> ( $x=0.15, 0.18, 0.22, 0.25$ ) (a) $x=0.15$ , (b) $x=0.18$ , (c) $x=0.22$ , (d) $x=0.25$ , (e) $x=0$

Fig. 2 shows the SEM images of commercial  $\beta$ -Ni(OH)<sub>2</sub> and Ni<sub>1-x</sub>Mn<sub>x</sub>(OH)<sub>2</sub> ( $x=0.15, 0.18, 0.22, 0.25$ ). As shown in the figures, commercial Ni(OH)<sub>2</sub> was composed of regular spherical particles, which became fine and irregular after doping with Mn. The porous structure produced by such fine particles can improve contact between the electrolyte and sample, thereby increasing the active material utilization rate of the sample [24] and improving the electrical properties of the sample. The more microstructural defects a sample material has, the more favorable it becomes for proton diffusion and charge transfer in the electrode process [25], thereby increasing the discharge specific capacity of the electrode material.

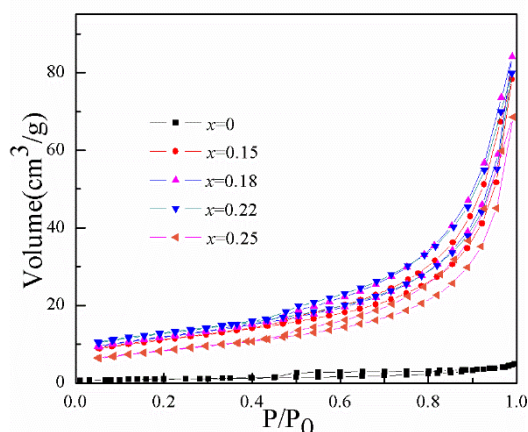


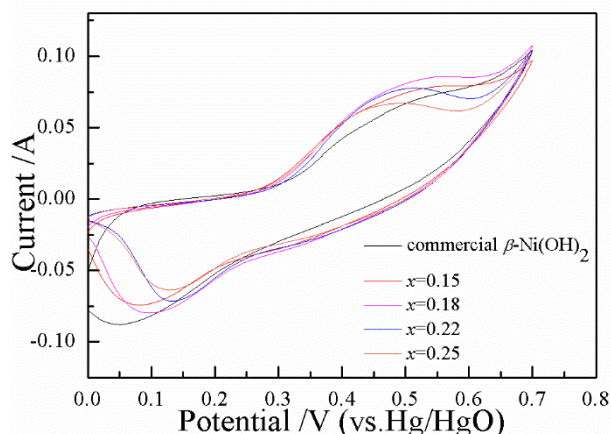
**Figure 3.** N<sub>2</sub> adsorption-desorption isotherms of commercial  $\beta$ -Ni(OH)<sub>2</sub> and Ni<sub>1-x</sub>Mn<sub>x</sub>(OH)<sub>2</sub>

The specific surface area measurements [26] results showed that  $S_{BET}$  ( $\beta$ -Ni(OH)<sub>2</sub>) was  $9 \text{ m}^2 \cdot \text{g}^{-1}$ ,  $S_{BET}$  ( $x=0.15$ ) was  $39 \text{ m}^2 \cdot \text{g}^{-1}$ ,  $S_{BET}$  ( $x=0.18$ ) was  $41 \text{ m}^2 \cdot \text{g}^{-1}$ ,  $S_{BET}$  ( $x=0.22$ ) was  $39 \text{ m}^2 \cdot \text{g}^{-1}$  and  $S_{BET}$  ( $x=0.25$ ) was  $36 \text{ m}^2 \cdot \text{g}^{-1}$ , the BET surface area of Mn-doped samples was more than that of commercial  $\beta$ -Ni(OH)<sub>2</sub>. Fig. 3 showed that the shape of the Mn-doped samples were all type IV curves. Hysteresis curves appeared at

P/P<sub>0</sub> between 0.45 and 1.0, which proved that the Mn-doped samples had mesoporous structures, which was consistent with the SEM test results. The mesoporous structures can effectively increase the electrode/electrolyte interfacial area, improve the rapid transmission capacity of ions in the electrolyte during the circulation process, and help improve the rate performance of the electrode materials [27].

### 3.2 Electrochemical analysis

Fig. 4 shows the CV curves of commercial  $\beta$ -Ni(OH)<sub>2</sub> and Ni<sub>1-x</sub>Mn<sub>x</sub>(OH)<sub>2</sub> ( $x=0.15, 0.18, 0.22, 0.25$ ) at the scan rate of 0.5 mV·s<sup>-1</sup> and voltage range of 0–0.7 V (vs. Hg/HgO). The curves of the five samples showed a pair of redox peaks, which were consistent with a discharge platform in the constant current charge and discharge curve. Among the five curves, the integral area of the  $x=0.18$  curve was larger than those of the  $x=0.15$  and  $x=0$  curves, whereas the integral area of the  $x=0.22$  and  $x=0.25$  curves was slightly smaller. These results indicated that proper Mn doping could increase the specific capacity of Ni(OH)<sub>2</sub>. The difference  $\Delta E$  between the oxidation peak potential and the reduction peak potential reflects the reversibility of the electrochemical reaction; a high  $\Delta E$  indicates the poor reversibility of the electrode reaction [28]. As shown in Fig. 3,  $\Delta E$  of  $\beta$ -Ni(OH)<sub>2</sub> was 509 mV, which was larger than that of the Mn-doped sample (i.e., 467 mV [ $x=0.15$ ], 459 mV [ $x=0.18$ ], 383 mV [ $x=0.22$ ], and 367 mV [ $x=0.25$ ]). Thus, the reversibility of the Mn-doped electrode reaction was better than that of commercial  $\beta$ -Ni(OH)<sub>2</sub>.



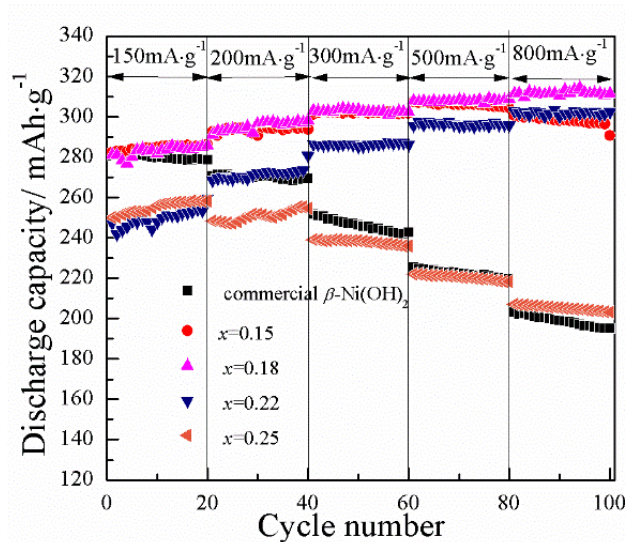
**Figure 4.** CV curves of commercial  $\beta$ -Ni(OH)<sub>2</sub> and Ni<sub>1-x</sub>Mn<sub>x</sub>(OH)<sub>2</sub> ( $x=0.15, 0.18, 0.22, 0.25$ ) at a scan rate of 0.5 mV·s<sup>-1</sup>

Fig. 5 shows the rate performance of commercial  $\beta$ -Ni(OH)<sub>2</sub> and Ni<sub>1-x</sub>Mn<sub>x</sub>(OH)<sub>2</sub> at the current densities of 150, 200, 300, 500, and 800 mA·g<sup>-1</sup>. Tab. 1 shows the comparison of discharge specific capacity of different electrode materials. As shown in Fig. 5,  $\beta$ -Ni(OH)<sub>2</sub> had the largest discharge specific capacity of 280.8 mAh·g<sup>-1</sup> at a current density of 150 mA·g<sup>-1</sup>. The discharge specific capacity was the smallest at 195 mAh·g<sup>-1</sup> under a current density of 800 mA·g<sup>-1</sup>. The discharge specific capacity

of the sample decreased with increasing current density, which was consistent with the reported trend [9], indicating that the large current discharge performance of commercial  $\beta$ -Ni(OH)<sub>2</sub> was poor. In the Ni<sub>1-x</sub>Mn<sub>x</sub>(OH)<sub>2</sub> sample, when  $x=0.15$  and the current density of the sample increased from 150 mA·g<sup>-1</sup> to 500 mA·g<sup>-1</sup>, the discharge specific capacity slowly increased to 303.4 mAh·g<sup>-1</sup>. The discharge specific capacity decreased slightly at a current density of 800 mA·g<sup>-1</sup>. When  $x=0.18$  and the current density of the sample increased from 150 mA·g<sup>-1</sup> to 800 mA·g<sup>-1</sup>, the discharge specific capacity increased slowly and peaked at 800 mA·g<sup>-1</sup>, which was 314.5 mAh·g<sup>-1</sup>. Compared with the electrode materials in Tab. 1, sample  $x=0.18$  had a higher specific discharge capacity. When the current density of the samples  $x=0.15$  and  $x=0.18$  was 150 mA·g<sup>-1</sup>, the discharge specific capacity was similar to that of commercial  $\beta$ -Ni(OH)<sub>2</sub>. When the current density increased from 200 mA·g<sup>-1</sup> to 800 mA·g<sup>-1</sup>, the discharge specific capacity was larger than that of commercial  $\beta$ -Ni(OH)<sub>2</sub>. When the current density of sample  $x=0.22$  increased from 150 mA·g<sup>-1</sup> to 800 mA·g<sup>-1</sup>, the discharge specific capacity increased slowly, reaching a maximum value of 308.2 mAh·g<sup>-1</sup> at 800 mA·g<sup>-1</sup>; its discharge specific capacity was slightly lower than that of sample  $x=0.18$  and larger than that of commercial  $\beta$ -Ni(OH)<sub>2</sub>. The trend of sample  $x=0.25$  was similar to that of commercial  $\beta$ -Ni(OH)<sub>2</sub>. The discharge specific capacity decreased with increasing current density. The maximum discharge specific capacity of sample  $x=0.25$  was 258.5 mAh·g<sup>-1</sup>, whereas its minimum discharge specific capacity was 203.2 mAh·g<sup>-1</sup>, with a 21.4% attenuation. Meanwhile, commercial  $\beta$ -Ni(OH)<sub>2</sub> decayed by 30.6% under the same conditions. The samples  $x=0.15$ ,  $x=0.18$ , and  $x=0.22$  showed that the discharge specific capacity increased with the increase in current density, and the active material of the positive electrode doped with Mn was activated slowly. One of the possible reasons for this finding is that the binder of the graphite emulsion may be hydrophobic, which affects the activation of the positive electrode active material. Another reason may be that the doped Mn is originally in a low-cost state and gradually transforms into a high-valence state during charge and discharge.

**Table 1.** Comparison of discharge specific capacity of different electrode materials

References	Electrode materials	Preparation method	discharge specific capacity/ mAh/g
Chang [9]	Mn-doped $\alpha$ -Ni(OH) <sub>2</sub>	A chemical coprecipitation	330
Wu [10]	Mn-doped Ni(OH) <sub>2</sub>	A chemical coprecipitation	270
Li [11]	Mn-doped $\beta$ -Ni(OH) <sub>2</sub>	Mechanical attrition method	261
Li [12]	Mn-Zn-doped Ni(OH) <sub>2</sub>	Mechanical attrition method	265
Wen [13]	Al-doped $\alpha$ -Ni(OH) <sub>2</sub>	A chemical coprecipitation	324
Bao [14]	Al-Cu-doped $\alpha$ -Ni(OH) <sub>2</sub>	Ultrasonic-assisted precipitation method	330
Xiao [16]	Mn-doped $\beta$ -Ni(OH) <sub>2</sub>	Buffer solution method	294



**Figure 5.** Rate performance of commercial  $\beta$ -Ni(OH)<sub>2</sub> and Ni<sub>1-x</sub>Mn<sub>x</sub>(OH)<sub>2</sub>

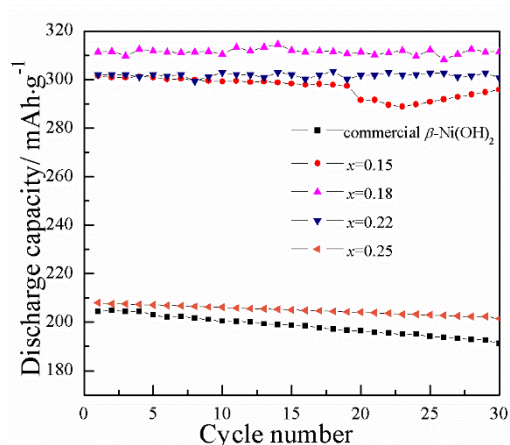


**Figure 6.** Cyclic performance of commercial  $\beta$ -Ni(OH)<sub>2</sub> and Ni<sub>1-x</sub>Mn<sub>x</sub>(OH)<sub>2</sub> at 800 mA·g<sup>-1</sup>

Fig. 6 shows the cyclic performance of commercial  $\beta$ -Ni(OH)<sub>2</sub> and Ni<sub>1-x</sub>Mn<sub>x</sub>(OH)<sub>2</sub> at 800 mA·g<sup>-1</sup>. As shown in Fig. 6, the Mn-doped sample presented better discharge performance and a higher discharge specific capacity than  $\beta$ -Ni(OH)<sub>2</sub>. The maximum discharge specific capacity of the  $\beta$ -Ni(OH)<sub>2</sub> sample was 204.9 mA·h·g<sup>-1</sup>, and the maximum discharge specific capacity of the sample  $x=0.18$  was 314.5 mA·h·g<sup>-1</sup>. The electrodes of Ni<sub>1-x</sub>Mn<sub>x</sub>(OH)<sub>2</sub> with different Mn contents showed a relatively stable cycle life. After 30 cycles, the discharge specific capacity of commercial  $\beta$ -Ni(OH)<sub>2</sub> decreased by 6.4%, whereas that of other Mn-doped samples decreased by 1.9% ( $x=0.15$ ), 0.49% ( $x=0.22$ ), and 3.1% ( $x=0.25$ ). When  $x=0.18$ , the discharge specific capacity of the samples did not decrease. Thus, Mn could effectively improve the discharge performance and cycle stability of the nickel electrode after replacing part of Ni.

Fig. 7 is a charge and discharge curve for the fifth cycle of commercial Ni(OH)<sub>2</sub> ( $x=0$ ) and Ni<sub>1-x</sub>Mn<sub>x</sub>(OH)<sub>2</sub> sample at a current density of 800 mA·g<sup>-1</sup>. In Fig. 7, an oblique line segment and charging platform were observed in the charging curve of each sample. The oblique line segment could be

considered a nickel electrode charging platform, and the high potential charging platform corresponded to the oxygen evolution side reaction. The oxidation reaction of Ni was mainly carried out in the early stage of charging, and the oxygen evolution reaction occurred in the late stage of charging. The oxygen evolution platforms of samples  $x=0.15$ ,  $x=0.18$ , and  $x=0.22$  were short, and the discharge specific capacity was high. When  $x=0.18$ , the maximum discharge specific capacity was  $311.8 \text{ mAh}\cdot\text{g}^{-1}$ . When  $x=0.15$ , the discharge specific capacity reached  $303.2 \text{ mAh}\cdot\text{g}^{-1}$ . When  $x=0.22$ , the discharge specific capacity reached  $301.9 \text{ mAh}\cdot\text{g}^{-1}$ . The samples  $x=0.25$  and  $x=0$  exhibited a long oxygen evolution platform, and the discharge specific capacity was low. When  $x=0.25$ , the discharge specific capacity reached  $204.2 \text{ mAh}\cdot\text{g}^{-1}$ . When  $x=0$ , the discharge specific capacity was  $202.5 \text{ mAh}\cdot\text{g}^{-1}$ . Thus, the oxygen evolution potential of Mn-doped samples was higher than that of commercial  $\beta\text{-Ni(OH)}_2$ . In the samples  $x=0.15$ ,  $x=0.18$ , and  $x=0.22$ , the charge median potential decreased and the difference between the oxygen evolution potential and the charge median potential increased, which facilitated the increase in charge efficiency [10] and improved the discharge capacity of samples.

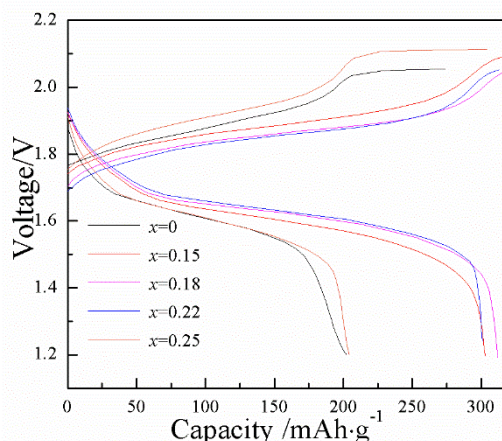


**Figure 7.** Charge-discharge curves of commercial  $\beta\text{-Ni(OH)}_2$  and  $\text{Ni}_{1-x}\text{Mn}_x(\text{OH})_2$  at current density of  $800 \text{ mA}\cdot\text{g}^{-1}$

#### 4. CONCLUSIONS

$\text{Ni}_{1-x}\text{Mn}_x(\text{OH})_2$  ( $x=0.15, 0.18, 0.22, 0.25$ ) cathode materials with different Mn contents were prepared by buffer solution method. The morphological characteristics and electrochemical properties of  $\text{Ni}_{1-x}\text{Mn}_x(\text{OH})_2$  were studied, and the following conclusions were drawn.

(1) XRD analysis showed that the  $\text{Ni}_{1-x}\text{Mn}_x(\text{OH})_2$  samples were all  $\beta$  phase, the samples  $x=0.18$ ,  $0.22$ ,  $0.25$  showed a heterogeneous phase, and the Mn-doped samples presented a narrow half-width and fine grains.

(2) The SEM test revealed that the Mn-doped sample was finer than the commercial  $\beta\text{-Ni(OH)}_2$  particles. The specific surface area measurements results showed that the BET surface area of Mn-doped samples were more and the Mn-doped samples had mesoporous structures.

(3) The CV test showed that the difference between the oxidation peak and the reduction peak potential of the Mn-doped sample was small, and the electrode reversibility was good.

(4) The discharge specific capacity of the Mn-doped sample increased first and then decreased with the increase in the Mn content. When  $x=0.18$ , the sample had a discharge specific capacity of  $314.5 \text{ mAh}\cdot\text{g}^{-1}$  at a current density of  $800 \text{ mA}\cdot\text{g}^{-1}$ , and the discharge specific capacity of commercial  $\beta$ -Ni(OH)<sub>2</sub> under the same conditions was  $195 \text{ mAh}\cdot\text{g}^{-1}$ . These results showed that doping Mn could increase the discharge specific capacity of nickel electrode and improve its current charge and discharge performance.

(5) When the Mn content was 0.18, the sample showed good cycle stability. The sample was circulated for 30 cycles under the same conditions. The discharge specific capacity was not attenuated when  $x=0.18$ , whereas the commercial Ni(OH)<sub>2</sub> was attenuated by 6.4%. The other samples were attenuated by 1.9% ( $x=0.15$ ), 0.49% ( $x=0.22$ ), and 3.1% ( $x=0.25$ ).

When the Mn content was 0.18 mol%, the discharge specific capacity of  $\beta$ -Ni(OH)<sub>2</sub> was effectively improved, which demonstrated enhanced electrochemical performance and cycle stability. Moreover, Mn replaced part of Ni, which greatly reduced the cost of the cathode material.

#### ACKNOWLEDGEMENTS

The authors acknowledge the financial support from the National Natural Science Foundation of China (No. 51776092).

#### References

1. S. Tan, D. J. Payne, J. P. Hallett, G. H. Kelsal, *Curr. Opin. Electrochem.*, 16(2019)83.
2. D. Rahangdale, A. Kumar, *J. Environ. Chem. Eng.*, 6(2018)1828.
3. K. Pourabdollah, *Chem. Eng. Sci.*, 160(2017)304.
4. S. Starborg, Y. Shen, D. Noréus, *Int. J. Hydrogen Engry*, 43(2018)18626.
5. J. Cheng, L. Zhang, Y.-S. Yang, Y.-H. Wen, G.-P. Cao, X.-D. Wang, *Electrochem. Commun.*, 9(2007)2639.
6. L. Zhang, J. Cheng, Y.-S. Yang, Y.-H. Wen, X.-D. Wang, G.-P. Cao, *J. Power Sources*, 179(2008)381.
7. J. Cheng, Y.-H. Wen, G.-P. Cao, Y.-S. Yang, *J. Power Sources*, 196(2011)1589.
8. S.-G. Yao, P. Liao, M. Xiao, J. Cheng, L. Xu, *Int. J. Electrochem. Sci.*, 5(2018)4455.
9. Y.-Q. Chang, Y.-L. Chen, H.-W. Wang, G.-R. Fu, X.-Q. Jin, L.-J. Xie, Z.-G. Hu, *New Chem. Mat.*, 39(2011)79.
10. M.-Y. Wu, J.-M. Wang, J.-Q. Zhang, C.-N. Cao, *Acta. Phys. Chim. Sin.*, 21(2005)523.
11. X.-F. Li, Z.-Li, H.-C. Dong, T.-C. Xia, *J. Zhengzhou Univ. Light Ind. (Nat. Sci. Ed.)*, 27(2012)7.
12. X.-F. Li, Z. Li, Y.-H. Song, H.-C. Dong, T.-C. Xia, *Chin. J. Power Sources*, 37(2013)240.
13. S.-S. Wen, X.-L. Liang, J.-H. Yao, G.-L. Pan, Y.-W. Li, L.-Z. Zhang, *Rare Met. Mater. Eng.*, 44(2015)3151.
14. J. Bao, Y.-J. Zhu, Y.-H. Zhuang, Q.-S. Xu, R.-D. Zhao, Y.-L. Liu, H.-L. Zhong, *T. Nonferr. Metal Soc.*, 23(2013)445.
15. J.-Y. Xue, W.-L. Ma, F.-M. Zhang, M.-M. Wang, H.-T. Cui, *Solid State Ionics*, 281(2015)38.
16. M. Xiao, R.-Y. Xing, S.-G. Yao, J. Cheng, Y.-J. Shen, Y.-S. Yang, *J. Inorg. Mater.*, 34(2019)703.
17. Y.-N. Zou, Y.-H. Cui, Z.-G. Zhou, P. Zan, Z.-X. Guo, M. Zhao, L. Ye, L.-J. Zhao, *J. Solid State Chem.*, 267(2018)53.

18. C.-C. Miao, Y.-J. Zhu, L.-G. Huang, T.-Q. Zhao, *J. Power Sources*, 274(2015)186.
19. Y. Pan, H. Lei, R.-G. Guo, X. Han, L.-M. Yu, W.-Q. Jiang, *Chem. Reagents*, 36(2014)949.
20. Y. Li, Y.-S. Xie, J.-H. Gong, Y.-F. Chen, Z.-T. Zhang. *Mater. Sci. Eng. B*, 86(2001)119.
21. S.-G. Yao, R.-Y. Xing, J. Cheng, M. Xiao, *Bat. Bim.*, 49(2019)182.
22. W.-G. Lv, J.-Y. Zheng, *Rare Metals Let.*, 24(2005)37.
23. R. W. Cheary, A. A. Coelho, *J. Appl. Crystallogr.*, 25(1992)109.
24. Y.-Z. Zhang, Y. Meng, Y.-J. Wang, L. Chen, Y. Guo, D. Xiao, *ChemElectroChem*, 4(2017)500.
25. J.-W. Chen, S.-H. Li, K. Qian, P.-S. Lee, *Mater. Today Energy*, 9(2018)74.
26. A.-J. Xu, B. Li, B.-S. Zhao, S.-X. Xue, R.-Q. Guo, W.-W. Zhong, *Int. J. Electrochem. Sci.*, 1(2017)448.
27. J.-X. Qiu, C. Lai, Y.-Z. Wang, S. Li, S.-Q. Zhang, *Chem. Eng. J.*, 256(2014)247.
28. C.-C. Zhang, X. Cai, D.-H. Xu, W.-Y. Chen, Y.-P. Fang, X.-Y. Yu, *Appl. Surf. Sci.*, 428(2018)73.

© 2020 The Authors. Published by ESG ([www.electrochemsci.org](http://www.electrochemsci.org)). This article is an open access article distributed under the terms and conditions of the Creative Commons Attribution license (<http://creativecommons.org/licenses/by/4.0/>).